



柔性微型无机发光二极管的瞬态传热分析

殷亚飞¹, 崔赟¹, 李宇航^{1,2*}, 邢誉峰¹

1. 北京航空航天大学固体力学研究所, 北京 100191

2. 西安交通大学航天航空学院机械结构强度与振动国家重点实验室, 西安 710049

* 通信作者. E-mail: liyuhang@buaa.edu.cn

收稿日期: 2018-03-22; 接受日期: 2018-05-09; 网络出版日期: 2018-06-11

国家重点基础研究发展计划 (批准号: 2015CB351900)、国家自然科学基金 (批准号: 11502009, 11772030) 和机械结构强度与振动国家重点实验室开放基金 (批准号: SV2018-KF-13) 资助项目

摘要 集成在柔性衬底上的微型无机发光二极管 (microscale inorganic light-emitting diodes, μ -ILED) 能够承受拉、弯、扭等载荷, 可以实现与人体组织直接集成, 可作为一种新型光学探测器应用于人体健康监测和临床医学诊断. 但这种电子器件在工作时会发出大量的热, 器件的传热特性成为应用的重要问题. 本文采用分离变量方法针对具有轴对称形状柔性 μ -ILED 瞬态传热过程建立了理论和有限元仿真模型, 得到了系统温升随时间和空间坐标的变化规律, 理论预测结果得到了有限元仿真的验证. 通过理论模型, 讨论了 μ -ILED 与封装层/衬底材料面内尺寸之间比值对正常工作下柔性 μ -ILED 温升的影响关系, 这些结果能够预测基于柔性 μ -ILED 的微小体征探测器的发热过程, 对其热管理及相应的散热设计具有一定的指导意义.

关键词 柔性微型无机发光二极管, 瞬态传热分析, 分离变量法

1 引言

近年来, 随着柔性电子技术的发展, 包括晶体管、发光二极管、天线、锂离子电池、传感器以及心脏起搏器在内的多种传统的刚性电子元器件都实现了柔性乃至可延展性^[1~9]. 相比于有机电子器件, 传统无机半导体材料具备更加优异的电子学性能, 同时由于其自身的脆性更难以实现柔性以及可延展性^[10]. 自2006年美国 University of Illinois 的 Rogers 教授和西北大学的黄永刚教授课题组提出通过屈曲力学设计提高无机半导体的材料拉伸能力以来^[11], 相关科研人员先后提出岛桥结构^[12]、蜿蜒桥结构^[13]、分形蜿蜒桥结构^[7, 14], 以及三维螺旋互联导线结构^[15]等一系列优化的结构力学设计, 为设计制备高性能柔性电子器件提供了理论依据.

在诸多柔性无机电子器件当中, 柔性微型无机发光二极管 (microscale inorganic light-emitting diodes, μ -ILED) 凭借自身效率高、寿命长、响应快以及良好的方向性等优势被广泛应用于柔性显

引用格式: 殷亚飞, 崔赟, 李宇航, 等. 柔性微型无机发光二极管的瞬态传热分析. 中国科学: 信息科学, 2018, 48: 734-742, doi: 10.1360/N112018-00056
Yin Y F, Cui Y, Li Y H, et al. A transient thermal analysis of microscale inorganic light-emitting diodes (in Chinese). Sci Sin Inform, 2018, 48: 734-742, doi: 10.1360/N112018-00056

示^[16], 加快生物伤口愈合以及动物大脑光遗传学^[4,5]的研究当中. 由于特殊的应用环境, 柔性 μ -ILED 尺寸极小 ($\sim 100 \mu\text{m} \times 100 \mu\text{m} \times 5 \mu\text{m}$ ^[2]), 在正常工作状态下就会引起较大的局部发热. 此外, 由于柔性衬底材料的热导率 ($\sim 0.1 \text{ W/m/K}$ ^[2,3]) 远低于传统的硅基芯片 ($\sim 100 \text{ W/m/K}$ ^[2,3]), 很难有效地将 LED 周围大量的局部发热传导出去, 从而导致 LED 温度急剧升高, 降低其发光效率甚至导致烧坏失效. 如果考虑到柔性 μ -ILED 与生物体乃至人体组织之间的集成, 对潜在的热损伤事故以及高温造成的不适感必须在器件设计时加以考虑.

针对以上提出的关于柔性 μ -ILED 发热管控问题, 相关科研工作者展开了大量的研究. 针对具有轴对称形状的柔性 μ -ILED, Lü 等^[17]建立了在恒定功率加载下的稳态传热理论和数值模型, 给出了无量纲 μ -ILED 温升仅依赖于 1 个无量纲参数的比例定律. 在此基础上, Li 等^[18,19]利用 Fourier 级数展开的方法研究了脉冲功率加载下柔性 μ -ILED 的热学性能, 给出了脉冲加载周期及占空比对柔性 μ -ILED 温升的影响并分析了插入动物大脑中柔性 μ -ILED 的热学行为. Cui 等^[20,21]将柔性 μ -ILED 的形状拓展到非轴对称形状下, 建立了矩形柔性 μ -ILED 的三维稳态传热模型, 通过叠加原理得到了多个 μ -ILED 共同作用下的温度场, 同时引入 Pennes 生物传热方程, 考虑了分别在恒定功率以及脉冲功率加载下矩形柔性 μ -ILED 与人体皮肤组织集成系统的传热性能和散热机制.

以上提到的理论模型均基于 Fourier 积分变换方法展开传热分析, 但是这种方法并不能够预测系统的瞬态加热过程; 同时这些研究都是基于衬底和封装层的面内尺寸远大于 μ -ILED 尺寸, 而将衬底和封装层的面内尺寸视为无限大的假设上, 没有将结构侧边的边界条件纳入考虑. 然而在一些应用中, 器件衬底和封装层的面内尺寸相对于 μ -ILED 的面内尺寸而言往往是有限的, 因此考虑衬底和封装的侧边边界条件是有必要的. 本文针对圆形柔性 μ -ILED, 考虑其面内尺寸与衬底和封装层面内尺寸基本相当的情况, 利用分离变量方法对其瞬态传热过程进行了理论建模并通过有限元仿真加以验证, 分析了 μ -ILED 与有限封装层/衬底材料面内尺寸之间比值对柔性 μ -ILED 温升的影响规律. 本文以下分 3 节内容进行介绍, 第 2 节给出了理论建模过程, 第 3 节对结果进行了分析、验证与讨论, 第 4 节对全文进行总结并给出了结论.

2 理论建模

图 1(a) 给出了一种典型的圆形柔性 μ -ILED 结构示意图, 将 μ -ILED 放置在水凝胶衬底材料上并通过 Su8 聚合物进行封装. 考虑到整个结构形状的对称性, 热传导问题可以简化成为一个轴对称模型加以分析. 如图 1(b) 所示是理论模型的示意图, 将坐标原点取于衬底材料下表面中心, r 表示面内半径方向, z 表示厚度方向. R 和 R_0 分别表示有限尺寸封装层/衬底材料以及 μ -ILED 的面内尺寸. H_e , H_L 以及 H_s 依次表示封装层、 μ -ILED 以及衬底层的厚度. 考虑到 μ -ILED 的面内尺寸 ($\sim 100 \mu\text{m}$) 往往远大于其厚度方向的尺寸 ($\sim 5 \mu\text{m}$), 因此热流主要通过其上下表面进行传递, 在理论模型中可以将 μ -ILED 视为一个没有厚度的, 位于封装层/衬底层界面上的一个面热源, 其热流密度的大小可近似表示为 $Q_0 = P/\pi R_0^2$, 其中 P 为 μ -ILED 的产热功率.

系统中的温度场为 $T(r, z, t)$, 令系统温升为 $\theta = T - T_\infty$, 则其满足如下轴对称热传导方程:

$$\begin{cases} \frac{\partial \theta_1}{\partial t} = \alpha_1 \left(\frac{\partial^2 \theta_1}{\partial r^2} + \frac{1}{r} \frac{\partial \theta_1}{\partial r} + \frac{\partial^2 \theta_1}{\partial z^2} \right), & 0 < z < H_s, 0 < r < R, \\ \frac{\partial \theta_2}{\partial t} = \alpha_2 \left(\frac{\partial^2 \theta_2}{\partial r^2} + \frac{1}{r} \frac{\partial \theta_2}{\partial r} + \frac{\partial^2 \theta_2}{\partial z^2} \right) + \frac{\alpha_2}{k_2} Q, & H_s < z < H_s + H_e, 0 < r < R, \end{cases} \quad (1)$$

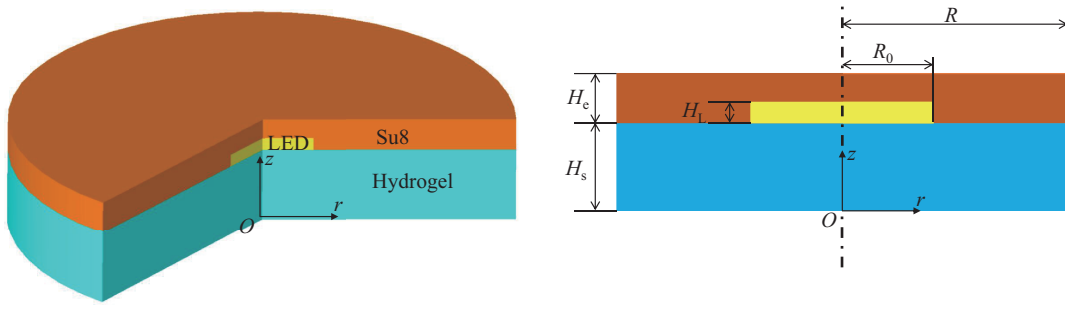


图 1 (网络版彩图) (a) 柔性 μ -ILED 结构示意图; (b) 轴对称理论模型示意图

Figure 1 (Color online) A schematic of (a) the μ -ILED structure; (b) the axisymmetric analytical model

其中 k 为热传导系数, α 为热扩散系数, 下标 1, 2 分别代表衬底层和封装层. Q 为 μ -ILED 处的热流密度, 可表示为 [22]

$$Q = Q_0 Q_1(r) Q_2(z) Q_3(t), \quad (2)$$

其中

$$Q_1(r) = \begin{cases} 1, & r \leq R_0, \\ 0, & R_0 < r \leq R, \end{cases} \quad (3)$$

$$Q_2(z) = \delta(z - H_s). \quad (4)$$

系统衬下方 ($z = 0$) 为常温条件, 封装层上表面 ($z = H_s + H_e$) 以及整个结构侧边的自然对流换热条件能够近似视作绝热条件 [17], 即

$$\theta_1|_{z=0} = 0, \quad (5a)$$

$$-k_2 \frac{\partial \theta_2}{\partial z} \Big|_{z=H_s+H_e} = 0, \quad (5b)$$

$$k_i \frac{\partial \theta_i}{\partial r} \Big|_{r=R} = 0, \quad i = 1, 2. \quad (5c)$$

在封装层/衬底材料界面上满足温度和热流的连续性条件:

$$\theta_1|_{z=H_s^-} = \theta_2|_{z=H_s^+}, \quad k_1 \frac{\partial \theta_1}{\partial z} \Big|_{z=H_s^-} = k_2 \frac{\partial \theta_2}{\partial z} \Big|_{z=H_s^+}. \quad (6)$$

初始条件为

$$\theta_i|_{t=0} = 0, \quad i = 1, 2. \quad (7)$$

考虑到式 (1) 中的热传导方程存在非齐次项, 利用分离变量方法首先考虑齐次形式的控制方程

$$\frac{\partial \theta_i}{\partial t} = \alpha_i \left(\frac{\partial^2 \theta_i}{\partial r^2} + \frac{1}{r} \frac{\partial \theta_i}{\partial r} + \frac{\partial^2 \theta_i}{\partial z^2} \right), \quad i = 1, 2. \quad (8)$$

通过分离变量方法将温升表示为如下形式:

$$\theta_i(r, z, t) = \psi(r) Z_i(z) Y(t), \quad i = 1, 2. \quad (9)$$

将式 (9) 代入式 (8) 以及边界条件式 (5) 和 (6) 可以得到如下几个分问题: 对于 $\psi(r)$, 其满足

$$\frac{1}{\psi(r)} \left(\frac{\partial^2 \psi(r)}{\partial r^2} + \frac{1}{r} \frac{\partial \psi(r)}{\partial r} \right) = -\eta^2, \quad 0 < r < R, \quad (10a)$$

$$\frac{\partial \psi}{\partial r} \Big|_{r=R} = 0. \quad (10b)$$

$Z_i(z)$ 满足

$$\begin{cases} \frac{1}{Z_1(z)} \frac{\partial^2 Z_1(z)}{\partial z^2} = -\gamma^2, \\ \frac{1}{Z_2(z)} \frac{\partial^2 Z_2(z)}{\partial z^2} = -\mu^2, \end{cases} \quad (11a)$$

$$\begin{cases} Z_1(z)|_{z=0} = 0, \\ Z_1(z)|_{z=H_s^-} = Z_2(z)|_{z=H_s^+}, \\ k_1 \frac{\partial Z_1(z)}{\partial z} \Big|_{z=H_s^-} = k_2 \frac{\partial Z_2(z)}{\partial z} \Big|_{z=H_s^+}, \\ -k_2 \frac{\partial Z_2(z)}{\partial z} \Big|_{z=H_s+H_e} = 0. \end{cases} \quad (11b)$$

而 $Y(t)$ 则满足

$$\frac{1}{Y(t)} \frac{\partial Y(t)}{\partial t} = -\lambda^2. \quad (12)$$

式 (10)~(12) 中各系数之间满足

$$\lambda^2 = \alpha_1 (\eta^2 + \gamma^2) = \alpha_2 (\eta^2 + \mu^2). \quad (13)$$

由于 $r=0$ 处的温升为有限值^[22], 因此 $\psi(r)$ 可以表示成为

$$\psi(r) = J_0(\eta_m r), \quad (14)$$

其中 η_m 是 $J_1(\eta_m R) = 0$ 的解.

根据式 (11), 可以得到

$$\begin{cases} Z_1(\gamma_n, z) = \sin(\gamma_n z), \\ Z_2(\mu_n, z) = \frac{\sin(\gamma_n H_s)}{\cos(\mu_n H_e)} \cos(\mu_n (H_s + H_e - z)), \end{cases} \quad (15)$$

其中特征值 μ_n 以及 γ_n 满足

$$\begin{vmatrix} \sin(\gamma_n H_s) & -\cos(\mu_n H_s) & -\sin(\mu_n H_s) \\ \cos(\gamma_n H_s) k_1 \gamma_n & \sin(\mu_n H_s) k_2 \mu_n & -\cos(\mu_n H_s) k_2 \mu_n \\ 0 & -\sin(\mu_n (H_s + H_e)) & \cos(\mu_n (H_s + H_e)) \end{vmatrix} = 0, \quad (16)$$

此外, 根据式 (13) 可以得到

$$\lambda_{mn}^2 = \alpha_1 (\eta_m^2 + \gamma_n^2) = \alpha_2 (\eta_m^2 + \mu_n^2). \quad (17)$$

由式 (16) 和 (17) 可以确定特征值 μ_n 以及 γ_n , 显然这两个特征值与 η_m 相关, 并不是独立的. 根据叠加原理可以得到

$$\begin{cases} \theta_1(r, z, t) = \sum_{m=1}^{\infty} \sum_{n=1}^{\infty} \psi(\eta_m, r) Z_1(\gamma_n, z) Y(t), \\ \theta_2(r, z, t) = \sum_{m=1}^{\infty} \sum_{n=1}^{\infty} \psi(\eta_m, r) Z_2(\mu_n, z) Y(t). \end{cases} \quad (18)$$

式 (18) 满足边界条件, 但并不满足式 (1) 中的控制方程以及初始条件, 将其代入式 (1) 得到

$$\begin{cases} \sum_{m=1}^{\infty} \sum_{n=1}^{\infty} \psi(\eta_m, r) Z_1(\gamma_n, z) \left[\frac{\partial Y(t)}{\partial t} + \lambda_{mn}^2 Y(t) \right] = 0, \\ \sum_{m=1}^{\infty} \sum_{n=1}^{\infty} \psi(\eta_m, r) Z_2(\mu_n, z) \left[\frac{\partial Y(t)}{\partial t} + \lambda_{mn}^2 Y(t) \right] = \frac{\alpha_2}{k_2} Q, \end{cases} \quad (19)$$

根据固有函数的正交性, 对 (19) 方程组中两式分别作用算子 $\frac{k_1}{\alpha_1} \int_{r=0}^R \int_{z=0}^{H_s} r Z_1(\gamma_n, z) \psi(\eta_m, r) dz dr$ 以及 $\frac{k_2}{\alpha_2} \int_{r=0}^R \int_{z=H_s}^{H_s+H_e} r Z_2(\mu_n, z) \psi(\eta_m, r) dz dr$ 并相加可得

$$\frac{\partial Y(t)}{\partial t} + \lambda^2 Y(t) = \frac{F_m G_{mn}}{M_m N_{mn}} Q_0 Q_3(t), \quad (20)$$

其中,

$$\begin{cases} M_m = \int_{r=0}^R r \psi^2(\eta_m, r) dr, \\ N_{mn} = \frac{k_1}{\alpha_1} \int_{z=0}^{H_s} Z_1^2(\gamma_n, z) dz + \frac{k_2}{\alpha_2} \int_{z=H_s}^{H_s+H_e} Z_2^2(\mu_n, z) dz, \\ F_m = \int_{r=0}^R r \psi(\eta_m, r) Q_1(r) dr, \\ G_{mn} = \int_{z=H_s}^{H_s+H_e} Z_2(\mu_n, z) Q_2(z) dz, \end{cases} \quad (21)$$

式 (20) 的初始条件为 $Y(0) = 0$.

根据参数变易法对式 (20) 进行求解, 可以得到

$$Y(t) = \frac{Q_0 F_m G_{mn}}{M_m N_{mn}} P_{mn}(t), \quad (22)$$

其中,

$$P_{mn}(t) = \int_0^t Q_3(\tau) e^{-\lambda^2(t-\tau)} d\tau. \quad (23)$$

将式 (22) 代入式 (18) 可以得到系统内任意一点的瞬态温升解为

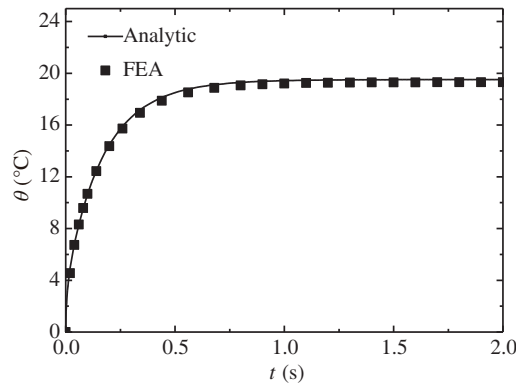
$$\begin{cases} \theta_1(r, z, t) = \sum_{m=1}^{\infty} \sum_{n=1}^{\infty} Q_0 \psi(\eta_m, r) Z_1(\gamma_n, z) \frac{F_m G_{mn}}{M_m N_{mn}} P_{mn}(t), \\ \theta_2(r, z, t) = \sum_{m=1}^{\infty} \sum_{n=1}^{\infty} Q_0 \psi(\eta_m, r) Z_2(\mu_n, z) \frac{F_m G_{mn}}{M_m N_{mn}} P_{mn}(t). \end{cases} \quad (24)$$

由于 μ -ILED 的热导率比封装层和衬底材料的热导率高出 3 个量级, 因此在整个 μ -ILED 处的温升趋于一致, 通过对封装层/衬底界面处的热源区域进行面积平均可以得到 μ -ILED 处的温升表达式

表 1 有限元仿真中各层材料的几何及材料参数 [8, 17~21]

Table 1 Geometric and material properties of each layer in finite element analysis [8, 17~21]

	Su8	μ -ILED	Hydrogel
Thickness (μm)	110	5	300
Radius (mm)	5	0.5	5
Density (kg/m^3)	1190	2329	1112
Conductivity ($\text{W}/\text{m}/\text{K}$)	0.2	160	0.6
Specific heat ($\text{J}/\text{kg}/\text{K}$)	1200	700	2375

图 2 μ -ILED 温升随时间的变化Figure 2 The time variation of the temperature increase of μ -ILED (FEA: finite element analysis)

如下:

$$\theta_{\text{LED}}(t) = \sum_{m=1}^{\infty} \sum_{n=1}^{\infty} Q_0 \psi_{\text{LED}}(\eta_m) Z_2(\mu_n, H_s) \frac{F_m G_{mn}}{M_m N_{mn}} P_{mn}(t), \quad (25)$$

其中,

$$\psi_{\text{LED}}(\eta_m) = \frac{2}{R_0^2} \int_0^{R_0} r \psi(\eta_m, r) dr. \quad (26)$$

3 结果与讨论

通过有限元软件 ABAQUS 建立系统的三维有限元模型, 上表面及侧边为自然对流条件, 下表面为常温条件, μ -ILED 上加载体热源, 采用 DC3D8 传热单元进行分析, 取加热功率为 50 mW, 有限元仿真中使用到的具体的几何以及材料参数如表 1 所示. 理论结果由式 (24) 和 (25) 所得, 其中考虑 μ -ILED 为恒定功率, 即

$$Q_3(t) = 1, \quad t > 0. \quad (27)$$

图 2 给出了由式 (25) 给出的 μ -ILED 处温升随时间的变化趋势, 理论预测值与有限元仿真结果吻合得很好. 从结果可以看出, 随着加热时间的增加, μ -ILED 处温升在 1 s 内迅速由初始的 0°C 增长到 19.2°C , 此后又经过 1 s 增长到 19.5°C , 加热 2 s 后 μ -ILED 温升基本达到稳态.

图 3 给出了系统在加热 10 s 达到稳态以后, 封装层/衬底材料界面内温升分布云图对比, 理论预测值同样得到了有限元仿真结果的验证. 从有限元结果图 3(b) 中可以看出, 在 μ -ILED 区域范围内温

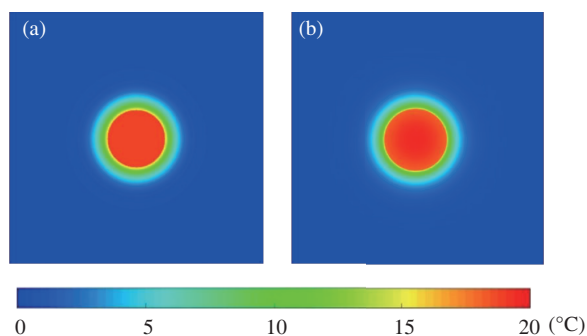


图 3 (网络版彩图) 封装层/衬底材料界面稳态温升分布图

Figure 3 (Color online) The distribution of the steady-state temperature increase at the encapsulation/substrate interface. (a) Analytic; (b) FEA

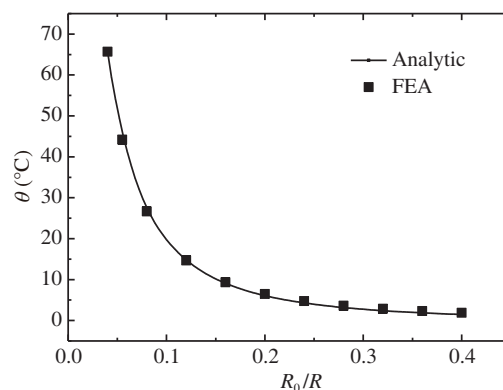


图 4 μ -ILED 稳态温升随面内尺寸比 R_0/R 的变化规律

Figure 4 The influence of the in-plane dimension ratio R_0/R on the steady-state temperature increase of μ -ILED

升几乎是完全平均化的,这也佐证了得到式(25)的面积平均方法的正确性.同时,在 μ -ILED区域以外,系统温度迅速衰减,由此可见,即便对于有限面内尺寸的情况,依然存在局部发热量较大的现象.

为了得到 μ -ILED与封装层/衬底材料面内尺寸相对大小对温度场的影响,图4给出了 μ -ILED稳态温升随热源与系统 r 方向尺寸比值 R_0/R 的变化规律.结果显示,在输入功率(50 mW)以及系统面内尺寸(5 mm)保持不变的情况下,随着 R_0/R 从0.04增加到0.4, μ -ILED处的稳态温升由 65.7°C 减小至 1.89°C .由此可见, μ -ILED与封装层/衬底材料面内尺寸逐渐接近能够有效地通过减小热流密度的方式减小 μ -ILED处的温升,对给定面内尺寸要求的器件,可以通过增加 μ -ILED的面内尺寸实现散热降温的作用.

4 结论

本文利用分离变量方法建立了圆形柔性 μ -ILED的瞬态传热理论模型并通过有限元仿真进行验证,解析得到了考虑有限面内尺寸情况下,系统温升随时间和空间坐标的变化规律.通过理论模型,分析了 μ -ILED与封装层/衬底材料面内尺寸之间比值对正常工作下柔性 μ -ILED稳态温升的影响规律,对器件散热机制提出了一种可行的建议,这对柔性 μ -ILED器件的热管理及相应的散热设计具有一定的指导意义.

参考文献

- 1 Kim D H, Ghaffari R, Lu N, et al. Flexible and stretchable electronics for biointegrated devices. *Annu Rev Biomed Eng*, 2012, 14: 113–128
- 2 Kim H S, Brueckner E, Song J, et al. Unusual strategies for using indium gallium nitride grown on silicon (111) for solid-state lighting. *Proc Natl Acad Sci USA*, 2011, 108: 10072–10077
- 3 Kim T I, Jung Y H, Song J, et al. High-efficiency, microscale GaN light-emitting diodes and their thermal properties on unusual substrates. *Small*, 2012, 8: 1643–1649
- 4 Kim R H, Tao H, Kim T I, et al. Materials and designs for wirelessly powered implantable light-emitting systems. *Small*, 2012, 8: 2812–2818

- 5 Kim T I, McCall J G, Jung Y H, et al. Injectable, cellular-scale optoelectronics with applications for wireless optogenetics. *Science*, 2013, 340: 211–216
- 6 Kim D H, Lu N, Ma R, et al. Epidermal electronics. *Science*, 2011, 333: 838–843
- 7 Xu S, Zhang Y, Cho J, et al. Stretchable batteries with self-similar serpentine interconnects and integrated wireless recharging systems. *Nat Commun*, 2013, 4: 1543
- 8 Chen Y, Lu B, Chen Y H, et al. Breathable and stretchable temperature sensors inspired by skin. *Sci Rep*, 2015, 5: 11505
- 9 Xu L, Gutbrod S R, Bonifas A P, et al. 3D multifunctional integumentary membranes for spatiotemporal cardiac measurements and stimulation across the entire epicardium. *Nat Commun*, 2014, 5: 3329
- 10 Huang Y, Li H C, Chen Y, et al. Stretchable and flexible photonics/electronics devices and transfer printing. *Sci Sin-Phys Mech Astron*, 2016, 46: 044607 [黄银, 李海成, 陈颖, 等. 可延展柔性光子/电子集成器件及转印技术. *中国科学:物理学 力学 天文学*, 2016, 46: 044607]
- 11 Khang D Y, Jiang H Q, Huang Y, et al. A stretchable form of single-crystal silicon for high-performance electronics on rubber substrates. *Science*, 2006, 311: 208–212
- 12 Ko H C, Stoykovich M P, Song J, et al. A hemispherical electronic eye camera based on compressible silicon optoelectronics. *Nature*, 2008, 454: 748–753
- 13 Kim D H, Song J, Choi W M, et al. Materials and noncoplanar mesh designs for integrated circuits with linear elastic responses to extreme mechanical deformations. *Proc Natl Acad Sci USA*, 2008, 105: 18675–18680
- 14 Zhang Y, Fu H, Su Y, et al. Mechanics of ultra-stretchable self-similar serpentine interconnects. *Acta Mater*, 2013, 61: 7816–7827
- 15 Jang K I, Li K, Chung H U, et al. Self-assembled three dimensional network designs for soft electronics. *Nat Commun*, 2017, 8: 15894
- 16 Park S I, Xiong Y, Kim R H, et al. Printed assemblies of inorganic light-emitting diodes for deformable and semi-transparent displays. *Science*, 2009, 325: 977–981
- 17 Lü C, Li Y, Song J, et al. A thermal analysis of the operation of microscale, inorganic light-emitting diodes. *Proc R Soc A-Math Phys Eng Sci*, 2012, 468: 3215–3223
- 18 Li Y, Shi Y, Song J, et al. Thermal properties of microscale inorganic light-emitting diodes in a pulsed operation. *J Appl Phys*, 2013, 113: 144505
- 19 Li Y, Shi X, Song J, et al. Thermal analysis of injectable, cellular-scale optoelectronics with pulsed power. *Proc R Soc A-Math Phys Eng Sci*, 2013, 469: 20130142
- 20 Cui Y, Li Y H, Xing Y F, et al. Thermal design of rectangular microscale inorganic light-emitting diodes. *Appl Thermal Eng*, 2017, 122: 653–660
- 21 Cui Y, Li Y H, Xing Y F, et al. Three-dimensional thermal analysis of rectangular micro-scale inorganic light-emitting diodes integrated with human skin. *Int J Thermal Sci*, 2018, 127: 321–328
- 22 Sun Y X, Ma J X, Liu S B, et al. Analytical solution of transient heat conduction in a bi-layered circular plate irradiated by laser pulse. *Can J Phys*, 2016, 95: 322–330

A transient thermal analysis of microscale inorganic light-emitting diodes

Yafei YIN¹, Yun CUI¹, Yuhang LI^{1,2*} & Yufeng XING¹

1. *Institute of Solid Mechanics, Beihang University, Beijing 100191, China;*

2. *State Key Laboratory of Strength and Vibration of Mechanical Structures, School of Aerospace Engineering, Xi'an Jiaotong University, Xi'an 710049, China*

* Corresponding author. E-mail: liyuhang@buaa.edu.cn

Abstract Microscale inorganic light-emitting diodes (μ -ILEDs) that are integrated in flexible substrates are able to be deformed like a rubber band. Such flexible μ -ILEDs can be integrated with human tissue directly as a novel optical detector applied to human health monitoring and clinical diagnosis. However, large amounts of heat will be emitted when such devices are operating, and the heat-transfer characteristics of the device are critical for its applications. In this paper, an axial symmetry analytical model, validated by 3D finite-element analysis, is developed to describe the transient heat transfer process based on the separation variable method. Both the time and space variations of the temperature increase are obtained theoretically. According to the analytical model, the influence of the in-plane dimension ratio R_0/R on the steady-state temperature increase of the μ -ILED is discussed. These results are able to predict the heating process of flexible μ -ILEDs and also pave the basis for thermal management and relevant thermal design of flexible μ -ILEDs.

Keywords flexible microscale inorganic light-emitting diodes, transient thermal analysis, separation variable method



Yafei YIN was born in 1995. He received his Bachelor's degree from Beihang University in 2017. Currently, he is a Master's candidate at the Institute of Solid Mechanics, Beihang University, Beijing. His current research interest mainly focuses on the thermal management of flexible and stretchable electronics.



Yun CUI was born in 1991. He received his Master's degree from Beihang University in 2017. Currently, he is a doctoral candidate at the Institute of Solid Mechanics, Beihang University, Beijing. His current research interests include the thermal analysis and thermomechanics of flexible and stretchable electronics.



Yuhang LI was born in 1983. He received his Ph.D. degree from Harbin Institute of Technology in 2012. Currently, he is an associate professor of the "Zhuoyue" Program at the Institute of Solid Mechanics, Beihang University, Beijing. His current research interests include flexible and stretchable electronic devices, such as actuators and sensors.



Yufeng XING was born in 1964. He received his Ph.D. degree from Dalian University of Technology in 1992. He is the director of the Institute of Solid Mechanics and the chief of the Intelligent Materials and Structural Dynamics Laboratory, Beihang University, Beijing. His research interests include structural dynamics, computational solid mechanics, and structural mechanics of composite materials.